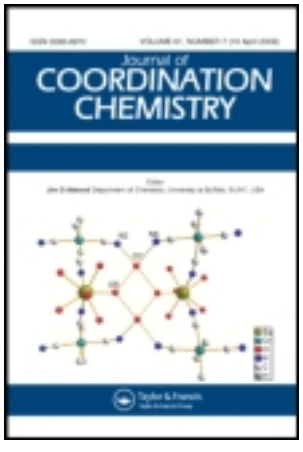

Journal of Coordination Chemistry
Publication details, including instructions for authors and subscription information:
http://www.tandfonline.com/loi/gcoo20

Linear hexadentate ligands as iron chelators

K.M. Clarke Jurchen & K.N. Raymond
[a] Department of Chemistry, University of California at Berkeley, CA 94720-1460, USA
Version of record first published: 25 Jan 2007.

To cite this article: K.M. Clarke Jurchen & K.N. Raymond (2005): Linear hexadentate ligands as iron chelators, Journal of Coordination Chemistry, 58:1, 55-80

To link to this article: http://dx.doi.org/10.1080/00958970512331328644

Journal of Coordination Chemistry
Vol. 58, No. 1, 10 January 2005, 55–80

Linear hexadentate ligands as iron chelators[†]

K.M. CLARKE JURCHEN and K.N. RAYMOND*

Department of Chemistry, University of California at Berkeley, CA 94720-1460, USA

(Received 13 October 2004; in final form 26 October 2004)

3LIHOPO$_2$TAM, 4LIHOPO$_2$TAM, 5LIHOPO$_2$TAM, 6LIHOPO$_2$TAM and 5LIOHOPO$_2$TAM represent a new class of linear, hexadentate hydroxypyridinone-containing ligands explored as iron(III) sequestering agents. The ligands incorporate the bifunctional 2,3-dihydroxyterephthalamide (TAM) unit as an integral part of the backbone linking two terminal 3,2-hydroxypyridinone (HOPO) units. The ferric complexes of 5LIHOPO$_2$TAM, 6LIHOPO$_2$TAM and 5LIOHOPO$_2$TAM have been prepared and structurally characterized by X-ray diffraction. Fe[5LIHOPO$_2$TAM] crystallizes in the triclinic space group $P\bar{1}$ with cell parameters $a = 12.4679(16)$, $b = 12.7498(16)$, $c = 15.1475(19)$ Å, $\alpha = 78.163(2)$, $\beta = 69.841(2)$, $\gamma = 89.671(2)^\circ$, $Z = 2$. Fe[6LIHOPO$_2$TAM] crystallizes in the monoclinic space group $I2/a$ with cell parameters $a = 28.1875(29)$, $b = 15.6457(16)$, $c = 22.6837(23)$ Å, $\beta = 90.080(2)^\circ$, $Z = 8$. Fe[5LIOHOPO$_2$TAM] crystallizes in the monoclinic space group $P2_1/c$ with cell parameters $a = 20.6200(19)$, $b = 9.2365(9)$, $c = 23.8669(22)$ Å, $\beta = 113.406(1)^\circ$, $Z = 4$. These ligands form mononuclear iron complexes with a ligand chirality independent of the metal center chirality. Fe[5LIOHOPO$_2$TAM] and Fe[5LIHOPO$_2$TAM] have different ligand chiralities for the same chirality metal center, and this difference is attributed to the effect of intramolecular hydrogen bonding between the ether oxygen and amide protons in 5LIOHOPO$_2$TAM. The aqueous coordination chemistry of 5LIOHOPO$_2$TAM with ferric ion has been examined using spectroscopic methods, giving a log formation constant of 32.1(1) (β_{110}) and a pM of 30.4 for ferric 5LIOHOPO$_2$TAM. The ferric complex stability is comparable to that of an analogous, previously described tripodal mixed terephthalamide/hydroxypyridinone ligand. The thermodynamic data validate the linear design strategy for this new class of hydroxypyridinone-containing ligands.

Keywords: Chelates of iron; Hexadentate ligands; Iron sequestering agents; Hydroxypyridinone-containing ligands; Iron(III) sequestering agents

1. Introduction

Iron is an essential nutrient whose dietary absorption and transport within the body is tightly regulated [1]. The human body has no established mechanism for iron excretion apart from blood loss. When iron intake exceeds iron loss, such as occurs in the treatment of the genetic blood disorder β-thalassemia, iron overload results [2]. This iron

[†]Dedicated to the late Professor Arthur E. Martell: scientist, friend and founder of this journal.
*Corresponding author. E-mail: Raymond@socrates.berkeley.edu

Journal of Coordination Chemistry
ISSN 0095-8972 print: ISSN 1029-0389 online
DOI: 10.1080/00958970512331328644

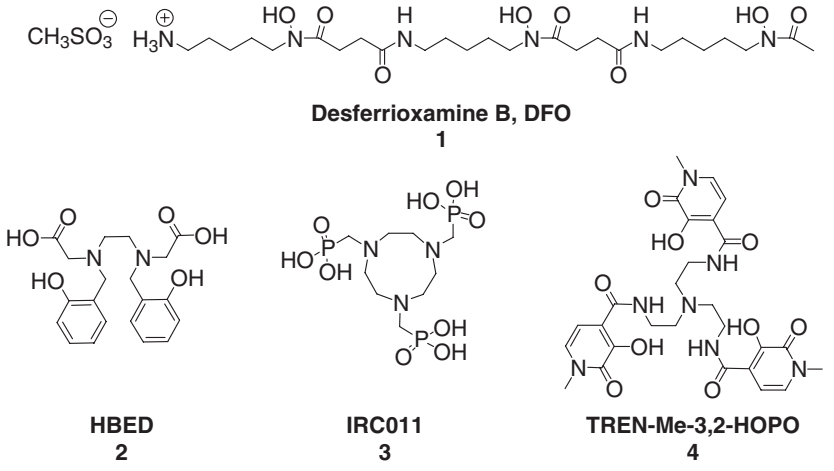

Figure 1. Linear desferrioxamine B and branched hexadentate chelators.

overload can be remediated by the administration of an organic ligand that is capable of binding iron *in vivo* and promoting its excretion as the iron complex. For the past 40 years, the naturally occurring siderophore desferrioxamine B (marketed under the name Desferal®) has been used for this purpose. Although it is effective in relieving iron overload, this therapy suffers from several drawbacks [3]. New, alternative iron chelation therapies are needed.

Desferrioxamine B contains three hydroxamate binding units arranged in a linear fashion along a single chain. By contrast, other hexadentate iron chelators currently under investigation for therapeutic use adopt a branched geometry (figure 1) [4–7], in which the chelating units are situated on arms branching from a central backbone. The effect of ligand geometry on chelation efficacy is not well understood, and it is possible that the linear geometry of desferrioxamine B may confer a therapeutic advantage. As a preliminary investigation of the effect of ligand geometry on therapeutic efficacy, a series of linear hexadentate ligands incorporating terephthalamide (TAM) and hydroxypyridinone (HOPO) binding units was prepared (figure 2).

The central design feature in these chelating agents takes advantage of the bifunctionality of 2,3-dihydroxyterephthalamide, which permits the attachment of alkylamine linkages to both carboxylate groups at the 1 and 4 positions on the binding unit. Additional chelating subunits, in this case HOPO, can then be attached via amide bonds to the alkylamine linkers, making the terephthalamide unit an integral part of the linker between two terminal hydroxypyridinone binding groups and affording a hexadentate ligand. This design has been used previously for the preparation of a mixed terephthalamide-hydroxamate siderophore analog [8] and a mixed terephthalamide-catecholate ligand briefly investigated as a potential therapeutic iron chelator [9]. A variety of different alkyl linkers was selected based on previous studies of tetradentate ligands with simple alkylamine linkers as potential actinide sequestering agents in mice, in which it was found that a small change in the linker, such as addition or removal of a methylene group, had a profound effect on the toxicity of the resulting ligand [10]. Therefore, four alkylamine linkers containing three to six methylene groups and one analogous linker containing a central ether group were chosen for additional studies toward the development of new chelating agents for iron.

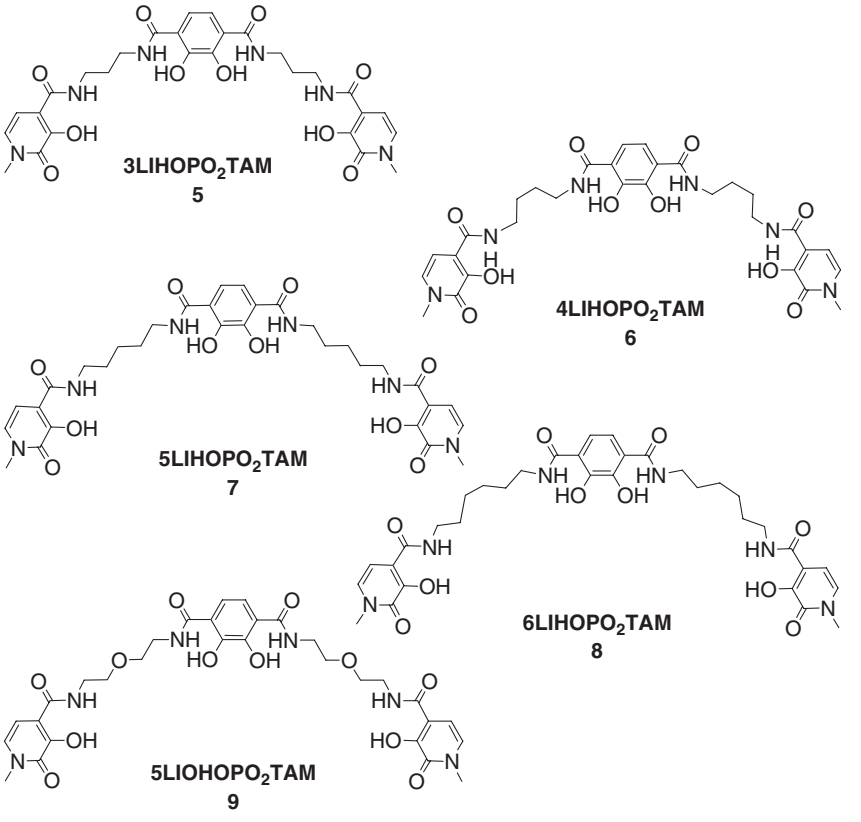

Figure 2. Linear ligand series.

The five linear hexadentate ligands in this series were each prepared using either of two synthetic strategies: a divergent strategy that builds outward from the central terephthalamide, and a convergent strategy that builds inward from the peripheral hydroxypyridinone units. The X-ray structures of three iron complexes in the series, confirming that these ligands form mononuclear iron complexes, are also described. The solution thermodynamic behavior of a representative ligand from this series was evaluated. These studies demonstrate that ligands constructed with linear geometries are capable of forming strong iron complexes, and show that the stability of these complexes is comparable to those of similar branched ligands that have been designed as potential therapeutic iron chelators.

2. Results and discussion

2.1 *Synthesis*

Terephthalamide and hydroxypyridinone binding subunits have been used as components of actinide decorporation agents [11,12], magnetic resonance imaging (MRI) contrast agents [13] and other potential therapeutic iron chelators [4,14], and the synthetic methodology for the preparation of ligands containing these subunits has been

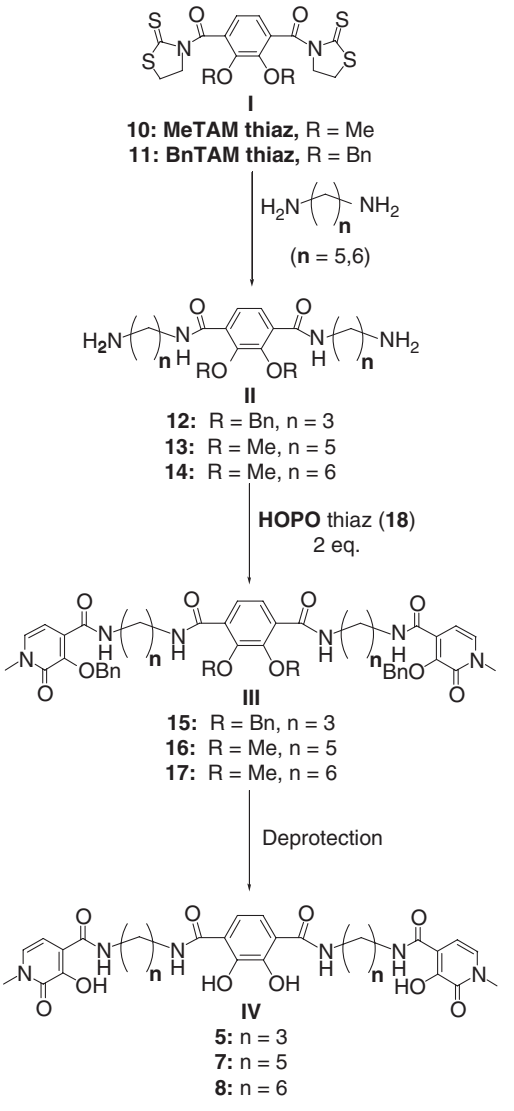

Scheme 1. Divergent synthetic strategy for linear ligands.

described previously. Schemes 1–3 show the synthetic strategies used in preparing the ligands in this series. For these syntheses, the binding subunits are added as the thiazolide-activated derivatives. Easily prepared and purified, these intermediates are stable in alcohols, water and dilute acids/bases, and can be stored for several months without degrading. The thiazolide-activated esters react selectively with primary amines to form amide products. The completion of the reaction is indicated by the disappearance of the characteristic yellow color of the intermediate [15,16]. The reaction produces the desired coupling product and free 2-mercaptothiazoline, which may be deprotonated and extracted from the organic product using a basic aqueous solution.

The results of the first coupling step (scheme 1) determine whether a ligand synthesis will proceed via the divergent or convergent pathway, with the deciding factor being the

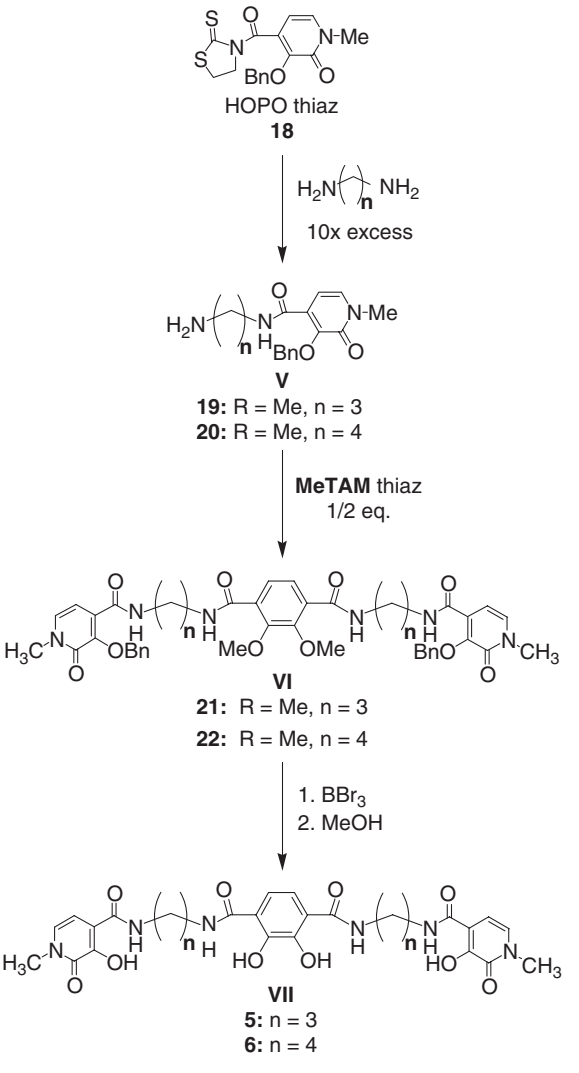

Scheme 2. Convergent synthetic strategy for linear ligands.

water solubility of the coupling product. In the first step of the divergent scheme, each activated amide group on the methyl- or benzyl-protected terephthalamide species **I** is coupled to a linear diamine using standard methodologies [17]. To avoid the formation of polymeric or oligomeric species, the reaction is performed in a 10-fold excess of the diamine to preserve the free amines in the desired product, **II**. Upon completion of the reaction, the excess water-soluble diamine may be removed from the product solution by aqueous extraction.

To complete the synthesis of the protected ligand, the free amine produced in the first coupling step (**II**) must be coupled to the terminal hydroxypyridinone binding groups. A slight excess of the thiazolide-activated HOPO derivative (HOPO thiaz, **18**) is added to a solution of the intermediate **II** to effect full coupling of the free amine ends. When the reaction is complete, the 2-mercaptothiazoline byproduct is again removed with

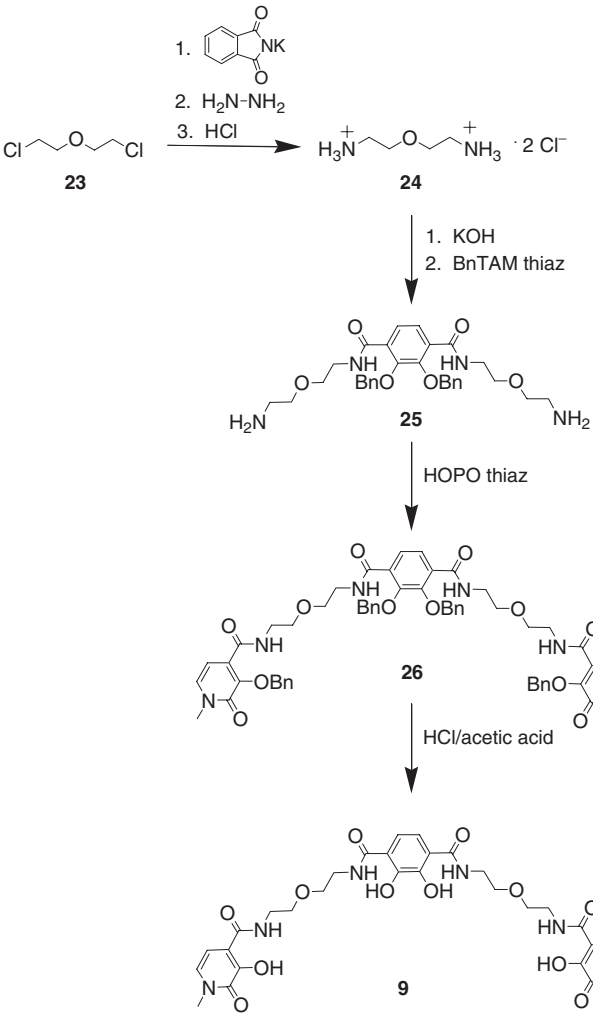

Scheme 3. Synthesis of 5LIOHOPO2TAM.

an aqueous base wash, and any unreacted **18**, which is much less polar than the coupled product **III**, is removed by flash silica column chromatography.

After the protected ligands have been synthesized and purified, the methyl and benzyl protecting groups are removed. When only benzyl protecting groups are present, they can easily be cleaved by treatment with strongly acidic conditions over a few hours. After the solvent is removed, the crude ligand is redissolved in a small amount of methanol and isolated by precipitation from ether. When methyl protecting groups are used, they must be removed by a harsher treatment with boron tribromide. To effect cleavage of these protecting groups, BBr_3 is added via syringe to solution of the protected ligand previously degassed by freeze–pump–thaw cycles. The solution is stirred for 3–5 days, at which time methanol is added to solvolyze the boron chelates and quench the remaining BBr_3. The methanol is distilled from the product solution, and volatile borate ester side products codistill with the methanol. When a flame test of drops of the distillate indicates that boron is no longer present (when boron is

present, the distillate gives a characteristic green flame), the product solution is allowed to cool. Upon cooling, the product usually precipitates, analytically pure, from the methanol solution.

It was found that when the 3LI or 4LI linkers were used in conjunction with methyl-protected TAM thiaz (**10**), the products of the first coupling reaction were water soluble, and were extracted into the aqueous phase with the excess diamine during purification. In these cases, the convergent synthetic strategy was used. The divergent strategy was used successfully to prepare 5LIHOPO$_2$TAM (**7**) and 6LIHOPO$_2$TAM (**8**). When the benzyl-protected TAM starting material **11** was used, it was also possible to prepare 3LIHOPO$_2$TAM (**5**) using this method. When preparing 5LIOHOPO$_2$TAM (**9**), a modified strategy was required, as it was necessary first to synthesize the diamine from 2,2′-dichlorodiethylether, using a literature procedure that yields the dihydrochloride salt of the diamine [18]. Prior to beginning the ligand synthesis, the ammonium chloride salt is neutralized by treatment with a stoichiometric amount of KOH. The remainder of the synthesis (scheme 2) follows the divergent synthetic strategy. Because ethers such as those found in the 5LIO linker are cleaved by treatment with BBr_3, benzyl protecting groups were used in the synthesis of 5LIOHOPO$_2$TAM (**9**).

3LIHOPO$_2$TAM (**5**) and 4LIHOPO$_2$TAM (**6**) were prepared using the convergent synthetic strategy (scheme 3). In the convergent strategy, the first coupling reaction is performed with the diamine linker and the terminal hydroxypyridinone group. Again, a large excess of the diamine is used to prevent coupling of the free amine end to form HOPO dimers. Because the product of this reaction, **V**, incorporates only one polar amine group, these products are much less water soluble than their divergent counterparts, and can be isolated by the standard aqueous washes.

The free amine **V** is then coupled to the central terephthalamide **I**. If the amine present is insufficient to completely couple the terephthalamide reagent, the product mixture from the reaction contains both mono- and bis-coupled terephthalamide species. This problem of incomplete coupling is minimized through slow addition of thiazolide-activated terephthalamide (**I**), allowing full coupling of the reagent present (monitored by the color change of the reaction) between additions. With this slow addition, the yield of bis-coupled product **VI** increases notably. The methyl and benzyl protecting groups are removed from the protected ligands by boron tribromide deprotection, and the compounds are purified in the same manner as described above for the divergent synthetic pathway.

To verify that these ligands are capable of binding ferric ion in discrete, nonpolymeric complexes, the iron(III) complexes of all ligands were prepared and characterized by mass spectrometry and UV/visible absorbance spectroscopy. Several iron complexes were also crystallized and structurally characterized.

The complexation reaction is carried out in much the same way for each individual synthesis. The ligand is suspended in methanol and treated with one equivalent of KOH. One equivalent of Fe(acac)$_3$ is then added to the ligand solution. Concentration of the complex solution and precipitation from ether or acetone affords the analytically pure metal complex.

2.2 *X-ray crystallography*

The stoichiometries of the iron complexes with the ligands 5LIHOPO$_2$TAM (**7**), 6LI HOPO$_2$TAM (**8**) and 5LIOHOPO$_2$TAM (**9**) were confirmed by X-ray crystallographic

analysis. These ligands form 1 : 1 iron complexes. In all three crystal structures, the potassium counterion is bound by ligand carbonyl groups and by crystallized solvent. In each case, the potassium is bridged to a symmetry-related potassium ion by either carbonyl or solvent oxygen atoms.

A unique ligand geometry is observed in these iron complexes. In each, the ligand adopts a spiral conformation, wrapping around the metal ion, rather than encapsulating the metal ion in a central cavity in the manner of tripodal or macrobicyclic ligands. Because the twist of the ligand's spiral can be either left-handed or right-handed, it is possible for the ligand to have a chirality that is independent of the lambda/delta chirality of the metal center. There is not yet a standard convention in the literature for reporting this sort of chirality, but the distinction between left-handed and right-handed twists can be considered as being similar to the distinction between *R* and *S* chiral centers in organic molecules. Thus, we will adapt the *R*/*S* nomenclature for this purpose. If the spiral of the ligand runs clockwise, the ligand chirality will be designated *R*; if the spiral runs counterclockwise, the ligand chirality will be designated *S* (figure 3).

Each of the linear ligand complexes has a preferred pairing of ligand and metal chiralities (for example, *S* ligand with Δ metal), and crystallizes as a racemic mixture of enantiomers with opposite ligand *and* metal chiralities (*S*/Δ with *R*/Λ, and *S*/Λ with *R*/Δ). In the case of Fe[6LIHOPO$_2$TAM], the preferred pairing is *S*/Δ and *R*/Λ (figure 4). The same preferred pairing is found in the crystal structure of Fe[5LIHOPO$_2$TAM] (figure 5); however, in Fe[5LIOHOPO$_2$TAM] the preferred pairing is *S*/Λ with *R*/Δ (figure 6). This means that the Fe[5LIHOPO$_2$TAM] and Fe[5LIOHOPO$_2$TAM] metal complexes are not superimposable (figure 7), even though the only difference between the two ligands is that the central atom

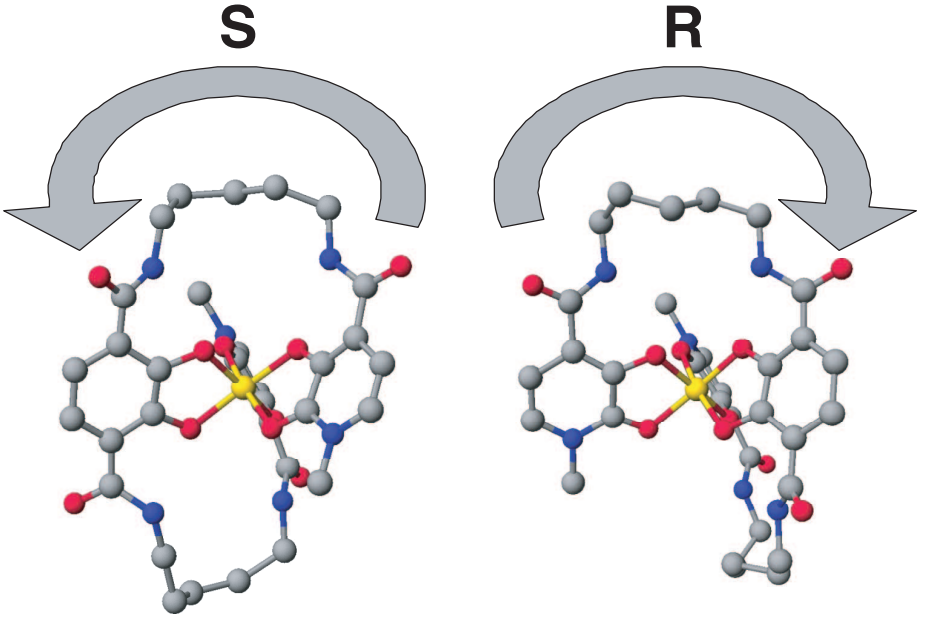

Figure 3. Molecular models showing *R* and *S* linear ligand chirality. Both are shown with a Δ metal center.

in the 5-atom linker is carbon in 5LIHOPO$_2$TAM and oxygen in 5LIOHOPO$_2$TAM. We can conclude that either hydrogen bonding to the ether oxygens in Fe[5LIOHOPO$_2$TAM] or steric crowding of the hydrogen atoms on the methylene group in Fe[5LIHOPO$_2$TAM] leads to this dramatic shift in ligand geometry.

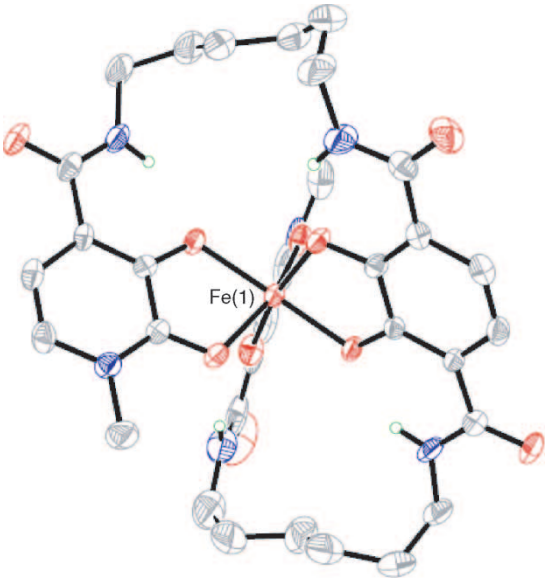

Figure 4. ORTEP diagram of Fe[6LIHOPO$_2$TAM]. Ellipsoids are shown at 50% probability. The R/Λ enantiomer is shown.

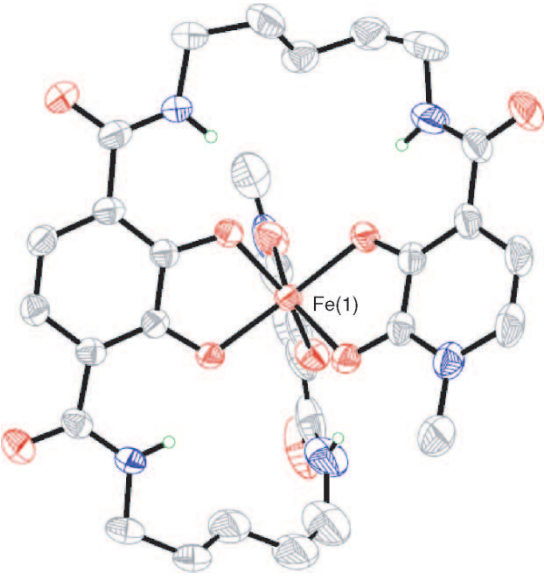

Figure 5. ORTEP diagram of Fe[5LIHOPO$_2$TAM]. Ellipsoids are shown at 50% probability. The S/Δ enantiomer is shown.

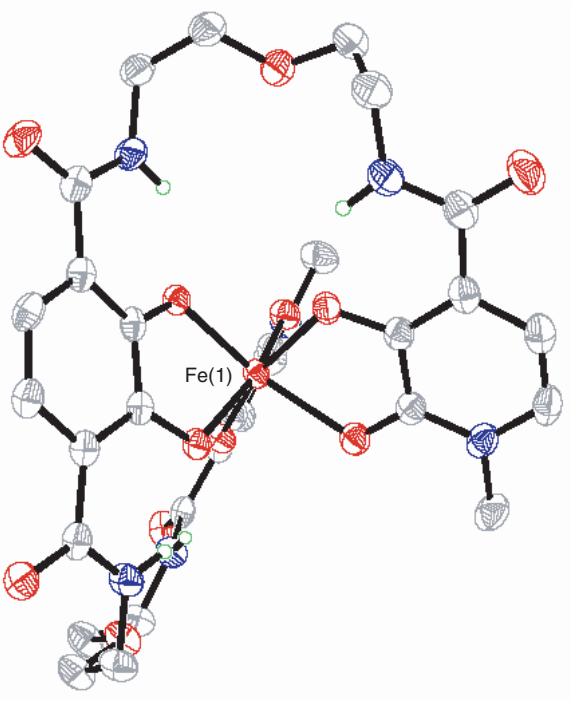

Figure 6. ORTEP diagram of Fe[5LIOHOPO$_2$TAM]. Ellipsoids are shown at 50% probability. The *S*/Λ enantiomer is shown.

It seems unlikely that the hydrogen atoms should present a steric hindrance in the extended paraffin structure exhibited by the 5LI linker chains. It is more likely that the root of the geometrical difference lies in hydrogen bonding to the 5LIO linker oxygens. An examination of amide–ether distances in Fe[5LIOHOPO$_2$TAM] bears out this hypothesis. The average N_{amide}–O_{ether} distance in Fe[5LIOHOPO$_2$TAM] is 2.88 Å, indicating the presence of a hydrogen bond [19]. This hydrogen bonding serves to draw the amide groups together. The amide–amide distances average 4.7 Å in Fe[5LIOHOPO$_2$TAM], shorter than the 5.1 Å average amide–amide distance in Fe[5LIHOPO$_2$TAM].

All three linear ligand complexes display the expected amide–phenol hydrogen bonding commonly observed in metal complexes containing terephthalamide and hydroxypyridinone groups [14]. In these complexes, the average N_{amide}–$O_{phenolate}$ distance is 2.7 Å, indicating a strong hydrogen-bonding interaction. These hydrogen bonds succeed in holding the amide groups near-planar with the aromatic TAM and HOPO rings; the average dihedral angle between the rings and the amide groups is 5.7°, 6.0° and 7.0° for Fe[6LIHOPO$_2$TAM], Fe[5LIHOPO$_2$TAM] and Fe[5LIOHOPO$_2$TAM], respectively.

A helpful tool in identifying geometric strain imposed by the ligand is the twist angle and comparison of this angle to the normalized bite [20]. The normalized bite for a bidentate binding unit is defined as normalized bite = (average Fe-binding atom distance)/(binding atom–binding atom distance). The twist angle is defined as the angle between the two Fe–O vectors in a binding unit projected onto a plane perpendicular

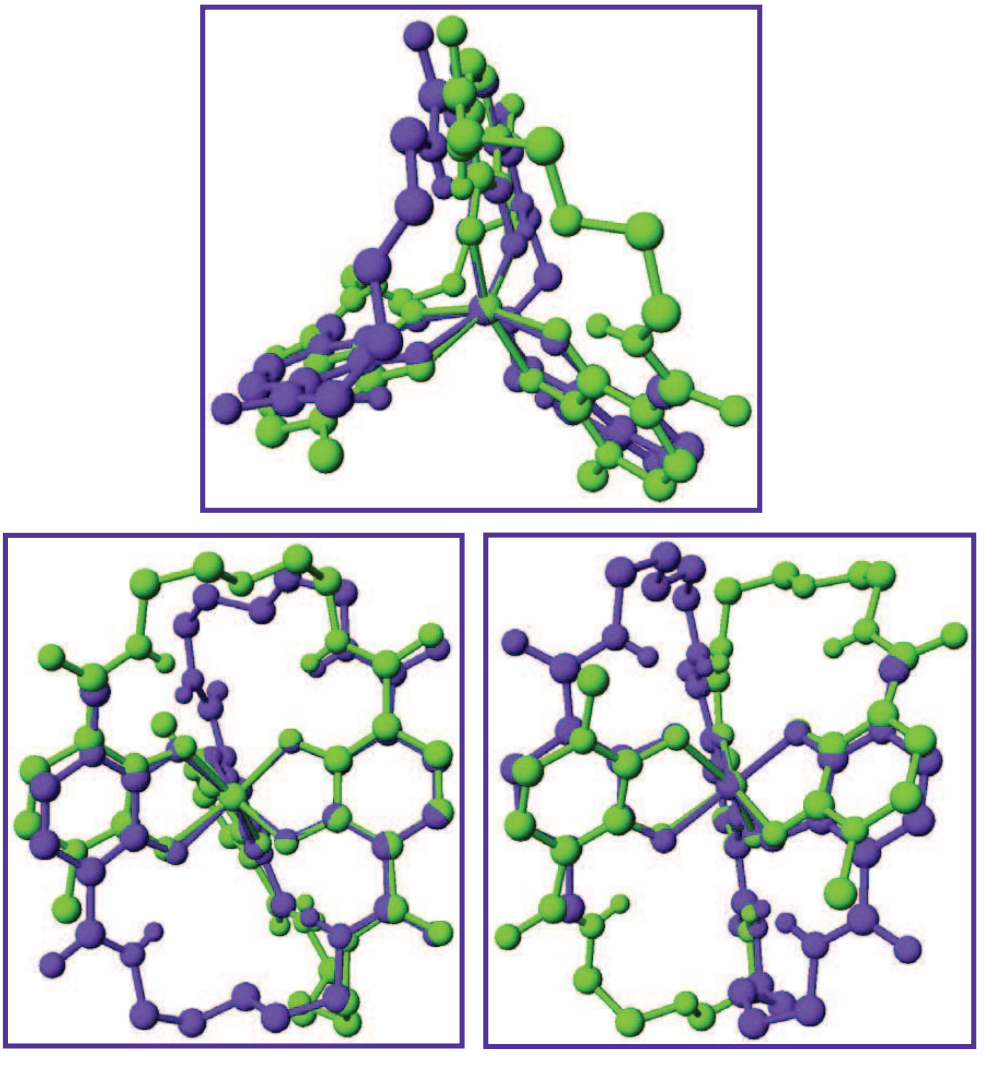

Figure 7. Three views of the semi-superimposed Fe[5LIHOPO$_2$TAM] and Fe[5LIOHOPO$_2$TAM] crystal structures showing different ligand chiralities for a Δ metal center. Fe[5LIHOPO$_2$TAM] is shown in blue, and Fe[5LIOHOPO$_2$TAM] is shown in green. The iron atoms and the terephthalamide phenolate oxygens are superimposed.

to the pseudo-threefold axis of the complex. The ideal twist angle for a spectrum of different normalized bites has been calculated [21], and these calculated twist angles correspond closely to those observed in actual tris-bidentate metal complexes. A linear relationship between normalized bite and twist angle over the usual range of normalized bites was determined by examination of several tris-bidentate metal complexes: twist angle $= (113^\circ \times \text{normalized bite}) - 102^\circ$ [22]. A large deviation between the ideal and actual twist angles for a complex provides notice of steric

constraints imposed by the ligand, and may indicate a thermodynamically less stable complex.

In comparing the match between normalized bite and twist angle for Fe[5LIO $HOPO_2$TAM] and Fe[5LIHOPO_2TAM], it is also helpful to look at the normalized bite and twist angle for Fe[6LIHOPO_2TAM]. The longer linkers in 6LIHOPO_2TAM provide more conformational flexibility, thus the twist angle in Fe[6LIHOPO_2TAM] should be very close to the ideal twist angle for these linear ligand complexes. In Fe[6LIHOPO_2TAM], the average normalized bite is 1.287, giving a calculated ideal twist angle of 43.39°. The actual average twist angle of the complex is 41.54°, indicating that the 6LIHOPO_2TAM ligand is able to easily adopt a conformation consistent with the ideal metal coordination geometry. Increasing amounts of strain are found in the Fe[5LIOHOPO_2TAM] complex and the Fe[5LIHOPO_2TAM] complex. The average normalized bite for Fe[5LIOHOPO_2TAM] is 1.276, which gives a calculated ideal twist angle of 42.15° for the complex. The actual twist angle at 37.36° is smaller than this ideal value, indicating that the ligand does impose some geometric constraints on the complex. The difference between the ideal and actual twist angle is relatively small, less than 5°, and so the ligand-imposed constraints can be considered to be minor. By contrast, the geometric constraints imposed by the 5LIHOPO_2TAM ligand would appear to be considerable. The normalized bite and ideal twist angle of Fe[5LIHOPO_2TAM] are the same as for Fe[5LIOHOPO_2TAM], 1.276 and 42.15°, while the actual twist angle at 30.25° deviates significantly from this ideal value. This may indicate that the Fe[5LIHOPO_2TAM] complex is less stable than the Fe[5LIOHOPO_2TAM] complex, due to increased geometric constraint imposed by the ligand.

2.3 *UV–visible spectra of iron complexes*

UV–visible spectra of the iron complexes can provide valuable insight into the stoichiometry of the iron complexes of the remaining members of this ligand series. This information is especially valuable, as the metal complexes may adopt one of two stoichiometries. If the linker between two binding groups is long enough, the ligand is able to wrap around a single metal ion, forming a 1 : 1 complex; however, if the linker is too short to allow the ligand to wrap around, complexes of higher stoichiometry, such as a 3 : 3 helicate, could result. In the former case, the UV–visible spectrum would indicate that the complex contains a mono-HOPO, bis-TAM iron center. In the latter case, the complex would contain two tris-HOPO centers and one tris-TAM center, and the spectrum should be a linear combination of purely HOPO and purely TAM spectra. Figure 8 shows both possibilities, in figure 8A the linear combinations of all-HOPO and all-TAM spectra, and in figure 8B the actual visual spectrum of ferric 5LIOHOPO_2TAM, confirmed by X-ray crystallography to be a mononuclear complex. The major difference between the (TAM + 2HOPO) linear combination spectrum and the actual Fe-5LIOHOPO_2TAM spectrum is that the peak at ~430 nm in the linear combination is well defined and separated from other peaks, while in the Fe-5LIOHOPO_2TAM spectrum this band is the shoulder of a larger peak below 400 nm. This difference can be used to distinguish between the two possible geometries for each linear ligand.

Figure 9 shows the visible spectra for the iron complexes of the linear ligand series. In each spectrum, the band at 410 nm appears to be a shoulder of a larger peak

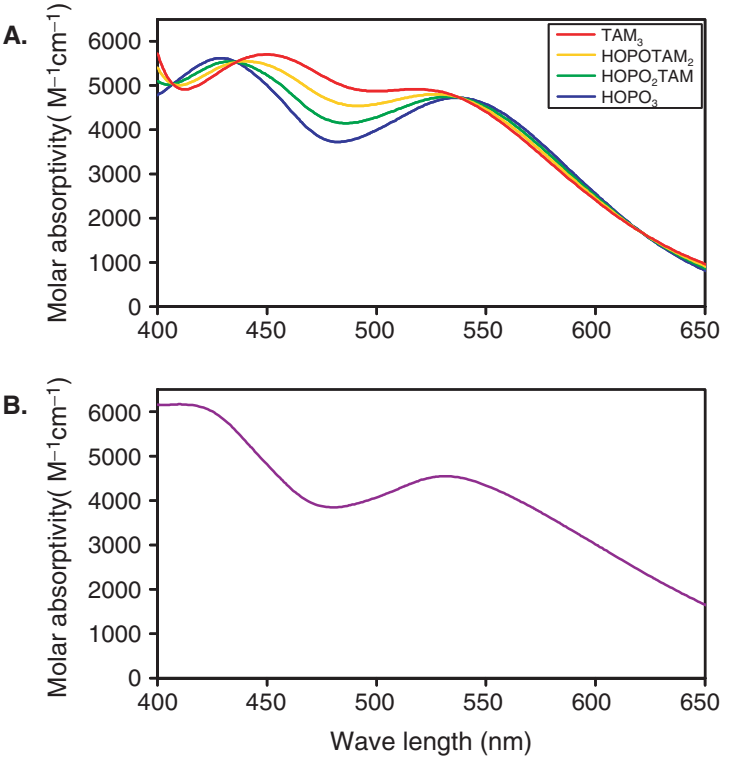

Figure 8. (A) Linear combinations of tris-TAM and tris-HOPO spectra. (B) Actual 5LIOHOPO$_2$TAM spectrum.

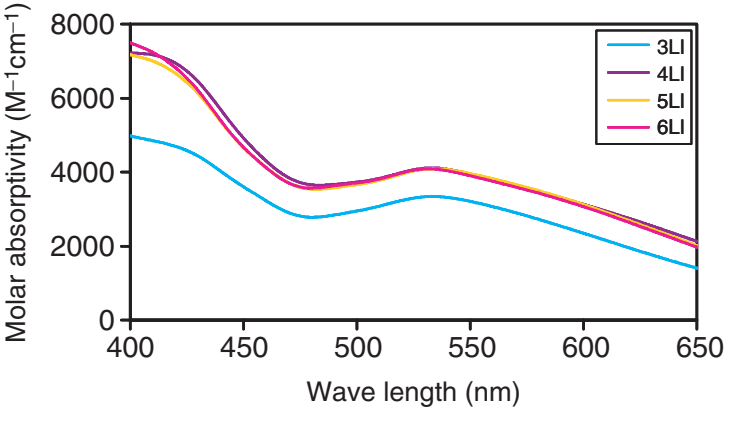

Figure 9. Linear *n*LIHOPO$_2$TAM iron complex spectra ($n = 3, 4, 5, 6$).

below 400 nm. This shape is more consistent with a mononuclear iron complex than with the proposed spectrum for a trinuclear iron complex. This evidence suggests that even the 3LI linker may be long enough to permit the ligand to wrap around a single metal center.

2.4 *Solution thermodynamics of 5LIOHOPO$_2$TAM*

Solution thermodynamic studies were performed on 5LIOHOPO$_2$TAM (**9**) as a representative member of this ligand series. The remaining ligands in the series were insufficiently soluble in aqueous solution for this purpose.

2.4.1 Protonation constants. The hexadentate ligand 5LIOHOPO$_2$TAM has four acidic protons, whose dissociation constants were determined by potentiometric titration. In this experiment, a constant buffering region was observed from pH 5 to 9, followed by a "jump" in which little buffering occurred, and another region of buffering near pH 10. Analysis of the titration curves indicated four sequential proton dissociation equilibria corresponding to pK_a values of 5.81(2), 6.54(2), 7.45(2) and 9.68(2) (figure 10) [23].

2.4.2 EDTA competition titrations. The most commonly used technique for determining the formation constant of iron complexes with strongly binding ligands is by competition titration with a ligand of known iron affinity [24]. EDTA is an ideal competitor for these experiments, as its protonation and iron complexation equilibria are well characterized, and both the ligand and its iron complex are transparent above 420 nm [25]. Thus, the equilibrium $FeEDTA^- + H_nL \leftrightarrows FeL^{(3-n)+} + H_2EDTA^{2-} + (n-2)H^+$ can be monitored at several different values of $[H^+]$ (i.e. pH) by recording the solution's absorbance at wavelengths between 420 and 650 nm, where charge-transfer bands give the HOPO and TAM iron complexes their red or purple color. For HOPO/TAM ligands, the above equilibrium is accessible in the general pH range 2.5 to 6.0.

Hexadentate 5LIOHOPO$_2$TAM is capable of saturating the octahedral coordination sphere of Fe(III), and 1 : 1 ligand–iron complexes are expected to be the only ones present in solution. For 5LIOHOPO$_2$TAM, the slow rate of the ligand exchange reaction necessitated the use of a batch titration technique, in which the pH of aliquots from a bulk solution are adjusted individually, and the aliquots are allowed to equilibrate for

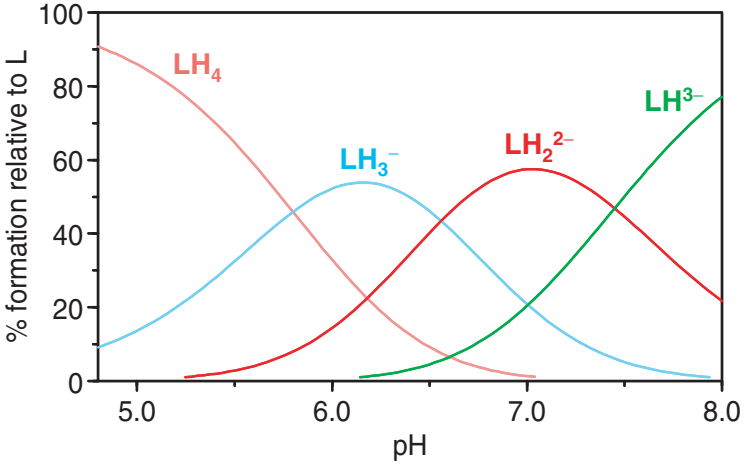

Figure 10. Speciation diagram for 5LIOHOPO$_2$TAM ligand.

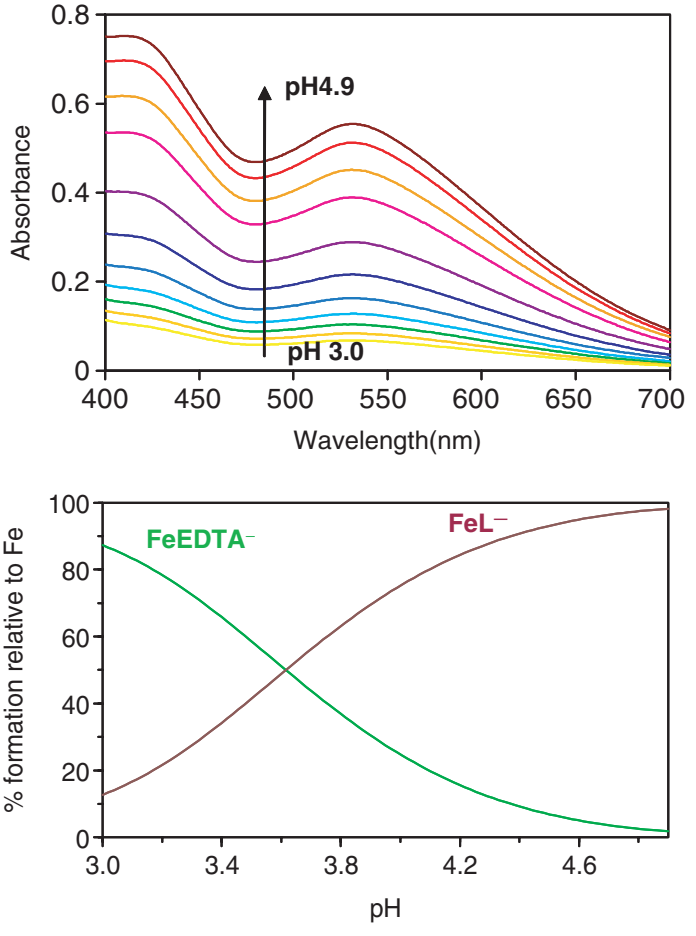

Figure 11. Sample 5LIOHOPO$_2$TAM EDTA competition spectra and corresponding speciation diagram.

48 h before UV–visible spectra are taken. Sample spectra and a speciation diagram calculated based on the Fe-5LIOHOPO$_2$TAM formation constant refined using these data are shown in figure 11. At low pH, the titration solution is colorless, indicating complete formation of the Fe-EDTA complex. As the pH is increased, the charge-transfer bands of the Fe-5LIHOPO$_2$TAM complex can be seen growing in at 411 and 531 nm. From these experiments, $\log \beta_{110}$ was found to be 32.1(1). Based on this value and the ligand protonation constants, the pM is calculated to be 30.4. The pM is defined as the negative log of the free iron concentration at physiological pH with 1 μm total iron concentration and 10 μm total ligand concentration. A higher pM indicates a stronger iron complex. Determination of the pM for this ligand makes it possible to compare the iron-binding effectiveness of these linear ligands with that of tripodal ligands studied earlier, as the solution thermodynamics of an analogous tripodal ligand containing one terephthalamide and two hydroxypyridinone groups, TREN-Me-3,2-HOPOTAM (figure 12), has been determined previously [14]. The pM for TREN-Me-3,2-HOPOTAM is 30.2, almost identical to the pM of 5LIOHOPO$_2$TAM, indicating that these ligands have nearly the same iron-binding

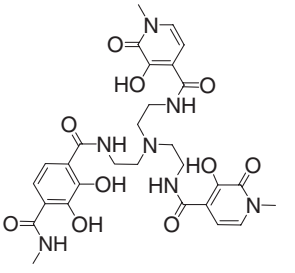

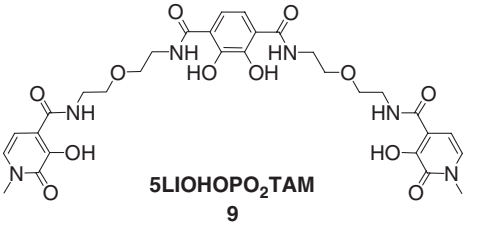

Figure 12. TREN-Me-3,2-HOPOTAM and 5LIOHOPO$_2$TAM: the two ligands contain the same bidentate chelating units but have different overall geometries.

ability at physiological pH and validating the linear design concept for this class of mixed terephthalamide/hydroxypyridinone ligands.

3. Conclusions

A series of ligands has been prepared that incorporate a linear geometry similar to desferrioxamine B. The linear hexadentate ligand design has been validated as one that produces stable iron complexes, as the pM of 5LIOHOPO$_2$TAM (**9**) is approximately equal to the pM of the analogous tripodal ligand TREN-Me-3,2-HOPOTAM. Structural studies of linear ligand iron complexes have confirmed that these ligands form mononuclear iron complexes, and have produced examples of a rarely seen ligand chirality that is independent of the chirality of the metal center. Hydrogen bonding to the ether oxygens in the 5LIO linker causes 5LIOHOPO$_2$TAM (**9**) to adopt a different geometry around the metal ion than the analogous 5LIHOPO$_2$TAM (**7**) ligand with an alkyl linker. UV–visible spectra of linear ligand iron complexes with shorter alkyl linkers suggest that these ligands with linkers as short as three atoms also form mononuclear complexes with iron.

4. Experimental

4.1 *Synthesis*

4.1.1 General. Unless otherwise noted, all reagents were obtained from commercial suppliers and used without further purification. All dropwise additions were performed under a N_2 atmosphere using a pressure-equalizing addition funnel. Organic solutions

were dried over anhydrous $MgSO_4$, and solvents were removed with a rotary evaporator. All chromatographic separations were performed using a 2 cm × 12 cm column of flash silica gel. Solutions were degassed by means of two or more freeze–pump–thaw cycles. ^{1}H NMR and proton-decoupled ^{13}C NMR spectra were obtained in $CDCl_3$ solutions using a Bruker FT-NMR spectrometer operating at 300 and 500 MHz, referenced to residual solvent protons. UV–visible spectra were recorded on a Cary UV–visible spectrophotometer as methanol solutions containing up to 30% water. Elemental analyses and mass spectrometry were performed in the Analytical Facility in the College of Chemistry at the University of California at Berkeley. The starting materials 3-benzyloxy-1-methyl-4-(2-thioxothiazolidin-1-yl)carbonyl-2(1H)-pyridinone (HOPO thiaz, **18**) [15,26], 2,3-dimethoxy-1,4-bis(2-thioxothiazolidin-1-yl) terephthalamide (MeTAM thiaz, **10**) [20] and 2,3-dibenzyloxy-1,4-bis(2-thioxothiazolidin-1-yl)terephthalamide (BnTAM thiaz, **11**) [27] were prepared according to procedures described in the literature.

4.2 *Preparation of 3LIHOPO$_2$TAM (5)*

4.2.1 Divergent synthesis

3LIBnTAM diamine (12). **11** (2.91 g, 5.01 mmol) was dissolved in CH_2Cl_2 (125 mL) and added dropwise to a solution of 1,3-diaminopropane (7.40 g, 100 mmol) in CH_2Cl_2 (15 mL). The final solution was washed with brine (40 mL) and 1 M KOH in brine (40 mL), dried and condensed to give a colorless oil that was used without further purification: ^{1}H NMR: δ 1.48 (quintet, $J = 6.7$, 4H, CH_2), 1.64 (s, br, 4H, NH_2), 2.61 (t, $J = 6.7$, 4H, CH_2), 3.35 (q, br, 4H, CH_2), 5.14 (s, 4H, $ArCH_2$), 7.38 (m, 10H, ArH), 7.87 (s, 2H, ArH), 7.89 (t, br, 2H, NH); ^{13}C NMR: δ 32.57, 37.39, 39.50, 76.80, 126.49, 128.47, 128.84, 128.92, 130.63, 135.73, 150.30, 164.31.

Protected 3LIHOPO$_2$TAM (15). **12** (2.24 g, 4.5 mmol) was dissolved in CH_2Cl_2 (75 mL). **18** (3.26 g, 9 mmol) was dissolved in CH_2Cl_2 (30 mL) and added to the amine solution. After 10 min, TLC (5% MeOH in CH_2Cl_2) of the reaction mixture showed product (baseline), excess **18** (R_f 0.1) and 2-mercaptothiazoline (R_f 0.15). The solution was washed with 1 M KOH in brine (2 × 40 mL), dried and condensed. The residue was applied to a silica column (2 × 20 cm) and eluted with 5% MeOH in CH_2Cl_2 to isolate the product. The product fractions were evaporated to dryness to yield a white foam (2.71 g, 55.7% from TAM thiaz); ^{1}H NMR: δ 1.38 (quintet, $J = 6.6$, 4H, CH_2), 3.15 (m, 8H, CH_2), 3.56 (s, 6H, CH_3), 5.13 (s, 4H, $ArCH_2$), 5.39 (s, 4H, $ArCH_2$), 6.72 (d, $J = 7.2$, 2H, ArH), 7.08 (d, $J = 7.2$, 2H, ArH), 7.29–7.41 (m, 20H, ArH), 7.77 (t, br, 2H, NH), 7.83 (s, 2H, ArH), 7.98 (t, br, 2H, NH); ^{13}C NMR: δ 29.01, 36.92, 36.98, 37.63, 74.80, 76.77, 104.78, 126.31, 128.55, 128.70, 127.78, 128.86, 129.01, 130.37, 130.75, 131.97, 135.75, 136.22, 146.43, 150.28, 159.53, 163.42, 164.43; Anal. Calc. (Found) for $C_{56}H_{56}N_6O_{10} \cdot CH_3OH$(%): C, 68.11 (68.05); H, 6.02 (5.92); N, 8.36 (8.46).

3LIHOPO$_2$TAM (5) by acid deprotection. **15** (2.71 g, 2.78 mmol) was dissolved in concentrated HCl (10 mL) and glacial acetic acid (10 mL). The flask was flushed with N_2 and the solution stirred overnight. The mixture was evaporated to dryness and coevaporated with MeOH (2 × 5 mL). The residue was suspended in methanol and heated to reflux, then cooled. The product was isolated by filtration as a white powder and rinsed with ether (1.38 g, 45.3% from TAM thiaz): ^{1}H NMR (DMSO-d_6): δ 1.78

(quintet, $J = 6.75$, 4H, CH_2), 3.33 (q, br, 8H, CH_2), 3.45 (s, 6H, CH_3), 6.51 (dd, $J = 20$, $J = 7.5$, 2H, ArH), 7.19 (dd, $J = 20$, $J = 7.5$, 2H, ArH), 7.30 (s, 2H, ArH), 8.53 (t, br, 2H, NH), 8.91 (t, br, 2H, NH), 11.69 (s, br, 2H, OH), 12.70 (s, br, 2H, OH); ^{13}C NMR (DMSO-d_6): δ 29.17, 37.23, 37.25, 37.30, 102.93, 116.01, 117.55, 117.61, 128.12, 148.08, 150.62, 158.45, 166.00, 169.13; Anal. Calc. (Found) for $C_{28}H_{32}N_6O_{10} \cdot 1.5H_2O$(%): C, 52.58 (52.61); H, 5.52 (5.64); N, 13.14 (13.20).

4.2.2 Convergent synthesis

3LIHOPO (19). A solution of **18** (1.81 g, 5.10 mmol) in dry CH_2Cl_2 (150 mL) was added dropwise to a solution of 1,3-diaminopropane (3.91 g, 52.8 mmol) in dry CH_2Cl_2 (50 mL). When addition was complete, the solution was washed with brine (100 mL) and 2 M KOH in brine (50 mL), dried, and condensed to give a light-colored oil (1.58 g) that was used *in situ* without further purification: ^{1}H NMR: δ 1.45 (quintet, $J = 6.6$, 4H, CH_2), 2.57 (t, $J = 6.6$, 2H, NH_2), 3.29 (q, $J = 6.9$, 2H, CH_2), 3.59 (s, 3H, CH_3), 5.37 (s, 2H, $ArCH_2$), 6.77 (d, $J = 7.2$, 1H, ArH), 7.11 (d, $J = 7.2$, 1H, ArH), 7.33–7.42 (m, 5H, ArH), 8.05 (s, br, 1H, NH); ^{13}C NMR: δ 32.56, 37.33, 37.68, 39.49, 74.90, 104.98, 128.78, 128.86, 129.03, 130.54, 132.03, 136.32, 146.52, 159.66, 163.29.

Protected 3LIHOPO$_2$TAM (21). **10** (1.07 g, 2.50 mmol) was added slowly to a solution of **19** (1.58 g, 5.01 mmol) in dry CH_2Cl_2 (125 mL). The flask was evacuated and flushed with N_2, and then heated to 35°C with stirring. After 30 min, the solution was allowed to cool, washed with brine (100 mL) and 1 M KOH in brine (2×50 mL), dried and condensed. The desired product was separated from unreacted **10** and side products by column chromatography, eluting with a gradient of 1–3% MeOH in CH_2Cl_2. The product fractions were condensed to yield an off-white solid (1.52 g) that was used *in situ*: ^{1}H NMR: δ 1.61 (quintet, $J = 6.6$, 4H, CH_2), 3.34 (quintet, $J = 6.6$, 8H, CH_2), 3.61 (s, 6H, CH_3), 3.97 (s, 6H, CH_3), 5.43 (s, 4H, $ArCH_2$), 6.77 (d, $J = 7.2$, 2H, ArH), 7.11 (d, $J = 7.2$, 2H, ArH), 7.35–7.45 (m, 10H, ArH), 7.86 (s, 2H, ArH), 8.05–8.08 (m, 4H, NH).

3LIHOPO$_2$TAM (5) by BBr$_3$ deprotection. A solution of **21** (1.52 g, 1.91 mmol) in CH_2Cl_2 (60 mL) was degassed and cooled to 195 K. BBr_3 (10.6 g, 42.3 mmol) was added with a gas-tight syringe. Immediate precipitation of a yellow solid produced a slurry, which was stirred for 5 days. MeOH was added to quench the remaining BBr_3. The CH_2Cl_2 and MeOH solvents were distilled to remove volatile methyl borate ester byproducts. When a flame test of the distillate indicated no boron was present, the solution was allowed to cool. Precipitation of a white solid accompanied cooling of the solution. The solid was collected by filtration and dried *in vacuo* to yield 0.958 g (62.0% overall): m.p. 239–240°C; ^{1}H NMR: (DMSO-d_6, 500 MHz): δ 1.79 (quintet, $J = 7$, 4H, CH_2), 3.32 (m, 8H, CH_2), 3.45 (s, 6H, CH_3), 6.49 (d, $J = 7.5$, 2H, ArH), 7.17 (d, $J = 7$, 2H, ArH), 7.29 (s, 2H, ArH), 8.51 (t, br, 2H, NH), 8.89 (t, br, 2H, NH); Anal. Calc. (Found) for $C_{28}H_{32}N_6O_{10} \cdot CH_3OH$(%): C, 54.03 (54.29); H, 5.63 (5.40); N, 13.04 (13.10).

4.3 *Preparation of 4LIHOPO$_2$TAM (6)*

4LIHOPO (20). To a solution of 1,4-diaminobutane (2.9 g, 0.033 mol) in CH_2Cl_2 (50 mL), **18** (1.20 g, 0.0033 mol) in CH_2Cl_2 (125 mL) was added dropwise. The resulting

solution was washed with 2 M KOH in brine (2 × 80 mL), dried and condensed to afford a pale oil, which was used in the next synthetic step: ^{1}H NMR δ 1.31–1.33 (m, 4H, CH_2), 1.70 (s, br, 2H, CH_2), 2.60 (t, $J = 6.6$, 2H, NH_2), 3.18–3.24 (m, 2H, CH_2), 3.59 (s, 3H, CH_3), 5.37 (s, 2H, CH_2), 6.78 (d, $J = 7.2$, 1H, ArH), 7.11 (d, $J = 7.2$, 1H, ArH), 7.35–7.46 (m, 5H, ArH), 7.96 (t, br, 1H, NH); ^{13}C NMR δ 26.3, 30.7, 37.7, 39.5, 41.6, 74.9, 104.9, 128.7, 128.8, 129.0, 130.5, 132.0, 136.2, 146.5, 159.6, 163.0.

4LIHOPO$_2$TAM, protected (22). **10** (0.51 g, 0.0012 mol) in CH_2Cl_2 (125 mL) was added dropwise to a CH_2Cl_2 (125 mL) solution of 20 from the previous reaction. The product solution was washed with 2 M KOH in brine (2 × 80 mL), dried and condensed. The product was separated from unreacted **10** by column chromatography, eluting with 3% MeOH in CH_2Cl_2, to afford 0.974 g (66.2% from **18**) of a colorless solid: ^{1}H NMR (500 MHz) δ 1.33–1.37 (m, 4H, CH_2), 1.42–1.46 (m, 4H, CH_2), 3.17–3.21 (m, 4H, CH_2), 3.31–3.35 (m, 4H, CH_2), 3.52 (s, 6H, CH_3), 3.84 (s, 6H, CH_3), 5.31 (s, 4H, CH_2), 6.69 (d, $J = 7.5$, 2H, ArH), 7.07 (d, $J = 7.5$, 2H, ArH), 7.27–7.38 (m, 10H, ArH), 7.72 (t, br, 2H, NH), 7.80 (s, 2H, ArH), 7.90 (t, br, 2H, NH); ^{13}C NMR δ 26.6, 26.9, 37.6, 39.3, 53.5, 61.5, 74.8, 104.7, 126.2, 128.7, 128.8, 128.9, 129.9, 130.3, 132.1, 136.1, 146.4, 151.3, 159.5, 163.1, 164.1; Anal. Calc. (Found) for $C_{46}H_{52}N_6O_{10} \cdot 1.5H_2O \cdot 0.5CH_3OH$(%): C 62.61 (62.72); H 6.44 (6.39); N 9.42 (9.45).

4LIHOPO$_2$TAM (6). **22** (0.974 g, 1.1 mmol) was dissolved in CH_2Cl_2 (50 mL) and the solution was degassed. BBr_3 (7.95 g, 31.7 mmol) was added via syringe, and the resulting slurry was stirred for 5 days. The reaction was quenched by slow addition of MeOH. The CH_2Cl_2 and MeOH solvents were distilled to remove volatile methyl borate ester byproducts. When a flame test of the distillate indicated no boron was present (no green flame), the solution was allowed to cool. The product precipitated upon cooling and was isolated by filtration to yield 0.574 g (53.9% from **18**) of an off-white solid: m.p. 230–235°C; ^{1}H NMR (DMSO-d_6): δ 1.55 (s, br, 8H, CH_2), 3.30 (s, br, 8H, CH_2), 3.44 (s, 6H, CH_3), 6.49 (d, $J = 7.5$, 2H, ArH), 7.16 (d, $J = 7.5$, 2H, ArH), 7.30 (s, 2H, ArH), 8.46 (t, $J = 5.5$, 2H, NH), 8.87 (t, $J = 5.5$, 2H, NH), 11.78 (s, br, 2H, OH), 12.79 (s, br, 2H, OH); ^{13}C NMR (DMSO-d_6): δ 26.69, 26.88, 37.22, 39.15, 102.77, 115.96, 117.36, 117.51, 128.09, 148.36, 150.72, 158.41, 166.09, 169.08; Anal. Calc. (Found) for $C_{30}H_{36}N_6O_{10} \cdot 2H_2O$(%): C 53.25 (53.27); H 5.96 (6.15); N 12.42 (12.72).

4.4 *Preparation of 5LIHOPO$_2$TAM (7)*

5LITAM (13). **10** (1.07 g, 2.50 mmol) was dissolved in dry CH_2Cl_2 (150 mL) and added dropwise to a solution of 1,5-diaminopentane (3.04 g, 29.8 mmol) in dry CH_2Cl_2 (50 mL). The product solution was washed with 2 M KOH in brine (2 × 50 mL), dried and condensed to yield a thick, light yellow–orange oil (0.818 g), which was used *in situ* without further purification: ^{1}H NMR (400 MHz): δ 1.45–1.51 (m, 12H, CH_2), 1.65 (quintet, $J = 6.8$, 4H, CH_2), 2.71 (t, $J = 6.8$, 4H, NH_2), 3.47 (q, $J = 6.8$, 4H, CH_2), 3.93 (s, 6H, CH_3), 7.81 (s, br, 2H, NH), 7.90 (s, 2H, ArH); ^{13}C NMR: δ 24.34, 29.45, 33.28, 39.69, 41.90, 61.57, 126.43, 129.99, 151.31, 164.08.

5LIHOPO$_2$TAM, protected (16). **13** (0.893 g, 2.26 mmol) was dissolved in dry CH_2Cl_2 (125 mL). To this solution was added 1.80 g of **18** (5.00 mmol). The reaction mixture was stirred under N_2 for 3 h, washed with 2 M KOH in brine (2 × 50 mL), dried and

condensed. The residue was applied to a silica gel column and eluted with 1% MeOH in CH_2Cl_2 to separate the product from unreacted **18**. Evaporation of the eluent yielded a pale, clear solid. The product was used without further purification in the next synthetic step: ^{1}H NMR δ 1.26–1.34 (m, 8H, CH_2), 1.49–1.53 (m, 4H, CH_2), 3.17 (q, $J = 6.5$, 4H, CH_2), 3.35 (q, $J = 6.5$, 4H, CH_2), 3.53 (s, 6H, CH_3), 3.86 (s, 6H, CH_3), 5.31 (s, 4H, CH_2), 6.68 (d, $J = 7$, 2H, ArH), 7.07 (d, $J = 7$, 2H, ArH), 7.29–7.39 (m, 10H, ArH), 7.73 (t, br, 2H, NH), 7.79 (s, 2H, ArH), 7.87 (t, br, 2H, NH); ^{13}C NMR: δ 24.21, 28.65, 29.02, 37.58, 39.38, 39.48, 61.53, 74.83, 104.74, 126.13, 128.72, 128.81, 128.91, 130.07, 130.33, 132.06, 136.16, 146.37, 151.26, 159.49, 163.05, 164.13; Anal. Calc. (Found) for $C_{48}H_{56}N_6O_{10} \cdot 2H_2O \cdot 0.5CH_3OH$(%): C 62.70 (62.83); H 6.73 (6.74); N 9.05 (9.05).

5LIHOPO$_2$TAM (7). **16** (1.8 g, 2.1 mmol) was dissolved in dry CH_2Cl_2 (60 mL), and the solution was degassed and cooled to 195 K. BBr_3 (10.6 g, 42.3 mmol) was added to this solution, producing a yellow suspension, which was stirred for 5 days. The reaction was quenched with MeOH, and the product was isolated as described above for **6**. Collection of the precipitate by filtration yielded 1.27 g of an off-white powder (72.3% from **10**): m.p. 113–120°C; ^{1}H NMR (DMSO-d_6): δ 1.33 (s, br, 4H, CH_2), 1.55 (s, br, 8H, CH_2), 3.27 (s, br, 8H, CH_2), 3.43 (s, 6H, CH_3), 6.48 (d, $J = 7$, 2H, ArH), 7.15 (d, $J = 7$, 2H, ArH), 7.29 (s, 2H, ArH), 8.44 (s, br, 2H, NH), 8.84 (s, br, 2H, NH); ^{13}C NMR (DMSO-d_6): δ 24.25, 28.82, 28.96, 37.21, 39.34, 102.74, 115.95, 117.33, 117.50, 128.06, 148.40, 150.70, 158.40, 166.08, 169.06; Anal. Calc. (Found) for $C_{32}H_{40}N_6O_{10} \cdot H_2O \cdot 0.5CH_3OH$(%): C 55.55 (55.70); H 6.31 (6.50); N 11.96 (11.92).

4.5 *Preparation of 6LIHOPO$_2$TAM (8)*

6LITAM (14). 1,6-Diaminohexane (5.65 g, 48.6 mmol) was dissolved in dry CH_2Cl_2 (50 mL). A solution of **10** (1.03 g, 2.40 mmol) in dry CH_2Cl_2 (175 mL) was added dropwise with stirring. The solution was washed with brine (100 mL), 1 M KOH in brine (2×80 mL) and distilled H_2O (2×30 mL), dried, and condensed to yield a pale oil (1.02 g), which was used without further purification in the next synthetic step: ^{1}H NMR: δ 1.38–1.49 (m, 16H, CH_2), 1.64 (quintet, $J = 6.6$, 4H, CH_2), 2.69 (t, $J = 6.9$, 4H, NH_2), 3.47 (q, $J = 6.9$, 4H, CH_2), 3.94 (s, 6H, CH_3), 7.80 (s, br, 2H, NH), 7.90 (s, 2H, ArH); ^{13}C NMR: δ 26.80, 27.16, 29.77, 33.91, 39.95, 42.36, 61.83, 126.45, 130.37, 151.61, 164.39.

Protected 6LIHOPO$_2$TAM (17). **14** (1.02 g, 2.40 mmol) was dissolved in dry CH_2Cl_2 (100 mL). **18** (1.73 g, 4.80 mmol) was added to the solution, and the reaction mixture was stirred for several hours. The solution was washed with brine (100 mL) and 1 M KOH in brine (2×100 mL), dried and condensed. The resulting yellow oil was applied to a silica gel column and eluted with 0.5% MeOH in CH_2Cl_2 to separate unreacted **18** from the product. Evaporation of the eluent yielded an off-white solid (1.30 g), which was used without further purification: ^{1}H NMR: δ 1.29 (m, 8H, CH_2), 1.59 (m, 8H, CH_2), 3.20 (q, $J = 6$, 4H, CH_2), 3.44 (q, $J = 5.7$, 4H, CH_2), 3.60 (s, 6H, CH_3), 3.94 (s, 6H, CH_3), 5.38 (s, 4H, $ArCH_2$), 6.79 (d, $J = 7.2$, 2H, ArH), 7.12 (d, $J = 7.2$, ArH), 7.34–7.42 (m, 10H, ArH), 7.78 (t, br, 2H, NH), 7.88–7.93 (m, 4H, ArH + NH).

6LIHOPO$_2$TAM (8). A solution of **17** (1.31 g, 1.44 mmol) in dry CH_2Cl_2 (75 mL) was degassed and cooled to 195 K. To this solution, 4.0 mL of BBr_3 (10.6 g, 42.3 mmol) was added using a gas-tight syringe. Immediate precipitation of a yellow solid produced a slurry, which was stirred for 5 days. The reaction was quenched with MeOH and the product was isolated as described above for **6**, providing 0.9 g (50% overall yield) of the desired product: m.p. 194–202°C; ^{1}H NMR (500 MHz, 10% MeOH-d_4 in $CDCl_3$): δ 1.36 (s, br, 8H, CH_2), 1.56 (s, br, 8H, CH_2), 3.35 (q, $J=7.5$, 8H, CH_2), 3.53 (s, 6H, CH_3), 3.57 (s, br, NH + OH), 6.72 (d, $J=7$, 2H, ArH), 6.83 (d, $J=7.5$, 2H, ArH), 7.16 (s, 2H, ArH), 7.95 (s, br, 2H, NH); ^{13}C NMR (10% MeOH-d_4 in $CDCl_3$): δ 26.13, 28.83, 28.89, 37.47, 39.27, 39.35, 105.60, 116.57, 117.95, 118.22, 126.96, 145.68, 148.50, 158.87, 164.30, 168.10; Anal. Calc. (Found) for $C_{34}H_{44}N_6O_{10}\cdot CH_3OH$(%): C, 57.68 (58.02); H, 6.64 (6.45); N, 11.53 (11.16).

4.6 *Preparation of 5LIOHOPO$_2$TAM (9)*

5LIOTAM amine (25). 5LIO amine dihydrochloride [18] (4.42 g, 0.025 mol) was dissolved in MeOH (50 mL) and deprotonated by the addition of 0.5 M KOH in MeOH (80 mL, 0.04 mol). **11** (1.45 g, 0.00250 mol) was dissolved in CH_2Cl_2 (125 mL) and added dropwise to the 5LIO amine solution. The reaction mixture was evaporated to dryness, redissolved in CH_2Cl_2 (150 mL), and washed with distilled water (20 mL) to remove excess 5LIO amine and 2 M KOH in brine (2×40 mL) to remove free 2-mercaptothiazoline. The resulting solution was dried over $MgSO_4$ and condensed to yield a pale yellow oil that was used without further purification in the next reaction: ^{1}H NMR: δ 2.75 (t, $J=5$, 4H, NH_2), 2.81 (q, br, 4H, CH_2), 3.37 (t, $J=5$, 4H, CH_2), 3.47 (t, $J=5$, 4H CH_2), 3.53 (t, $J=5$, 4H, CH_2), 5.11 (s, 4H, $ArCH_2$), 7.36 (m, 10H, ArH), 7.86 (s, 2H, ArH), 8.08 (t, br, 2H, NH); ^{13}C NMR: δ 39.59, 41.66, 53.42, 69.07, 73.07, 77.23, 126.53, 128.66, 128.70, 128.84, 130.66, 135.59, 150.39, 164.20.

5LIOHOPO$_2$TAM, Bn protected (26). **25** from the previous reaction (~2.5 mmol) was dissolved in CH_2Cl_2 (50 mL). **18** (1.80 g, 5.00 mmol) was dissolved in CH_2Cl_2 (30 mL) and added to the reaction mixture. The product solution was washed with 2 M KOH in brine (2×40 mL), dried and condensed. The residue was applied to a silica column (2×20 cm) and eluted with ethyl acetate to remove unreacted **18**; the product was then eluted with 10% MeOH in CH_2Cl_2. The product fractions were pooled and evaporated to dryness to yield **26** as a white foam (2.26 g, 87.4% over two steps): ^{1}H NMR: δ 3.23 (t, $J=5$, 4H, CH_2), 3.29 (m, 8H, CH_2), 3.34 (m, 4H, CH_2), 3.40 (s, 6H, CH_3), 4.98 (s, 4H, $ArCH_2$), 5.19 (s, 4H, $ArCH_2$), 6.61 (d, $J=7$, 2H, ArH), 6.98 (d, $J=7$, 2H, ArH), 7.21–7.31 (m, 20H, ArH), 7.72 (s, 2H, ArH), 7.83 (t, br, 2H, NH), 8.05 (t, br, 2H, NH); ^{13}C NMR: δ 37.50, 39.28, 39.42, 68.74, 68.92, 74.36, 76.93, 104.51, 126.06, 128.37, 128.54, 128.56, 128.60, 128.68, 128.90, 130.53, 130.81, 132.25, 135.81, 135.98, 146.11, 150.28, 159.32, 163.17, 164.45; Anal. Calc. (Found) for $C_{58}H_{60}N_6O_{12}\cdot CH_3OH$(%): C, 66.53 (66.27); H, 6.06 (6.06); N, 7.89 (7.97).

5LIOHOPO$_2$TAM (9). **26** (2.258 g, 2.186 mmol) was dissolved in glacial acetic acid (10 mL) and concentrated HCl (10 mL) and stirred overnight under a N_2 atmosphere. The solution was evaporated to dryness and coevaporated with MeOH (4×5 mL) to give an amber-colored foam. The product was redissolved in MeOH and precipitated upon standing to give the final ligand as a cream-colored powder (0.75 g, 43% from **11**): ^{1}H NMR (CD_3OD): δ 3.58 (s, 6H, CH_3), 3.59 (m, 8H, CH_2), 3.69 (m, 8H, CH_2), 6.69

(d, $J=7$, 2H, ArH), 7.08 (d, $J=7$, 2H, ArH), 7.11 (s, 2H, ArH); ^{13}C NMR: δ 37.10, 38.94, 39.16, 48.43, 68.36, 68.49, 105.10, 116.25, 117.71, 118.02, 127.52, 147.64, 148.62, 158.11, 166.25, 168.56; Anal. Calc. (Found) for $C_{30}H_{36}N_6O_{12} \cdot 1.5H_2O$(%): C, 51.50 (51.28); H, 5.62 (5.84); N, 12.01 (11.81).

4.7 *Iron complexes, general procedure*

A weighed portion of the ligand was dissolved in MeOH (10 mL) and degassed by applying a slight vacuum. KOH (0.5 M solution in MeOH) was added to the ligand solution with a glass syringe, and the solution was degassed again. Fe(acac)$_3$ was dissolved in MeOH (4 mL) and added to the ligand solution. The solution was degassed again and stirred for at least 1 h. The product solution was condensed to between 2 and 4 mL and added dropwise to 20–50 mL ether. The precipitated metal complex was isolated by centrifugation. After the supernatant was decanted, the solid was resuspended in 5 mL ether and collected by filtration.

Fe-3LIHOPO$_2$TAM. The complex was prepared as described above using **5** (0.19 g, 0.30 mmol), KOH (0.6 mL of a 0.5 M solution in MeOH, 0.3 mmol) and Fe(acac)$_3$ (0.106 g, 0.300 mmol). Yield 0.144 g, (61.9%): Anal. Calc. (Found) for $KC_{28}H_{28}N_6O_{10}Fe \cdot 4H_2O$(%): C, 43.36 (43.61); H, 4.68 (4.77); N, 10.84 (10.82). UV/vis: λ_{max} 273 nm (ε 2.72 $\times$ 10^4 M^{-1} cm^{-1}), 282 nm (ε 2.42 $\times$ 10^4 M^{-1} cm^{-1}), 337 nm (ε 1.39 $\times$ 10^4 M^{-1} cm^{-1}), 407 nm (ε 4.88 $\times$ 10^3 M^{-1} cm^{-1}), 531 nm (ε 3.34 $\times$ 10^3 M^{-1}cm^{-1}); ESI-MS m/z 664.3 (M$^-$).

Fe-4LIHOPO$_2$TAM. The complex was prepared as described above using **6** (0.129 g, 0.190 mmol), KOH (0.4 mL of a 0.5 M solution in MeOH, 0.2 mmol) and Fe(acac)$_3$ (0.0673 g, 0.190 mmol). Yield 0.125 g, (82.1%): Anal. Calc. (Found) for $KC_{30}H_{32}N_6O_{10}Fe \cdot 4H_2O$(%): C, 44.84 (44.53); H, 5.02 (4.90); N, 10.46 (10.46); UV/vis: λ_{max} 272 nm (ε 2.17 $\times$ 10^4 M^{-1} cm^{-1}), 340 nm (ε 1.60 $\times$ 10^4 M^{-1} cm^{-1}), 402 nm (ε 7.21 $\times$ 10^3 M^{-1} cm^{-1}), 533 nm (ε 4.11 $\times$ 10^3 M^{-1} cm^{-1}); ESI-MS m/z 692.2 (M$^-$).

Fe-5LIHOPO$_2$TAM. The complex was prepared as described above using **7** (0.136 g, 0.2 mmol), KOH (0.4 mL of a 0.5 M solution in MeOH, 0.2 mmol) and Fe(acac)$_3$ (0.071 g, 0.2 mmol). Yield 0.140 g (85.1%): Anal. Calc. (Found) for $KC_{32}H_{36}N_6O_{10}Fe \cdot 3.5H_2O$(%): C, 46.72 (46.75); H, 5.27 (4.91); N, 10.22 (9.74); UV/vis: λ_{max} 272 nm (ε 2.19 $\times$ 10^4 M^{-1} cm^{-1}), 338 nm (ε 1.54 $\times$ 10^4 M^{-1} cm^{-1}), 400 nm (ε 7.18 $\times$ 10^3 M^{-1} cm^{-1}), 534 nm (ε 4.10 $\times$ 10^3 M^{-1} cm^{-1}); ESI-MS m/z 720.3 (M$^-$).

Fe-6LIHOPO$_2$TAM. The complex was prepared as described above using **8** (0.140 g,0.200 mmol), KOH (0.4 mL of a 0.5 M solution in MeOH, 0.2 mmol) and Fe(acac)$_3$ (0.071 g, 0.20 mmol). Yield 0.149 g, (86.7%): Anal. Calc. (Found) for $KC_{34}H_{40}N_6O_{10}Fe \cdot 4H_2O$(%): C, 47.50 (47.29); H, 5.63 (5.68); N, 9.78 (9.44); UV/vis: λ_{max} 272 nm (ε 2.45 $\times$ 10^4 M^{-1} cm^{-1}), 281 nm (ε 2.13 $\times$ 10^4 M^{-1} cm^{-1}), 338 nm (ε 1.66 $\times$ 10^4 M^{-1} cm^{-1}), 402 nm (ε 7.45 $\times$ 10^3 M^{-1} cm^{-1}), 531 nm (ε 4.09 $\times$ 10^3 M^{-1} cm^{-1}); ESI-MS m/z 748.2 (M$^-$).

Fe-5LIOHOPO$_2$TAM. The complex was prepared as described above using **9** (0.140 g, 0.200 mmol), KOH (0.4 mL of a 0.5 M solution in MeOH, 0.2 mmol) and Fe(acac)$_3$ (0.071 g, 0.20 mmol). Yield 0.159 g, (97.2%): Anal. Calc. (Found) for $KC_{30}H_{32}N_6O_{12}Fe \cdot 3H_2O$(%): C, 44.07 (43.93); H, 4.68 (4.66); N, 10.28 (9.94);

UV/vis: λ_{max} 334 nm (ε $1.35 \times 10^4\ M^{-1}\,cm^{-1}$), 531 nm ($\varepsilon$ $4.54 \times 10^3\ M^{-1}\,cm^{-1}$); ESI-MS m/z 724.2 (M^-).

4.8 *Solution thermodynamics of 5LIOHOPO$_2$TAM*

4.8.1 General. The titration apparatus has been described in detail by O'Sullivan and coworkers [14,28,29]. Corning high-performance combination glass electrodes, whose response to [H^+] was calibrated before each titration [30], were used in concert with a Metrohm Titrino apparatus to measure the pH of the experimental solutions. Metrohm Titrino autoburets were used for incremental addition of acid or base standard solutions to the titration cell. The titration instruments were fully automated and controlled using LabView software [31]. Titrations were performed in 0.1 M KCl supporting electrolyte under positive Ar gas pressure. The temperature of the experimental solution was maintained at 25°C by an external circulating water bath. UV–visible spectra for batch titrations were recorded on a Varian Cary 300 Scan UV–visible spectrophotometer. Solid reagents were weighed on a Metrohm analytical balance accurate to 0.05 mg. Milli-Q purified water was used to prepare all solutions, and was degassed prior to use by simultaneously boiling and purging with Ar gas. Standard solutions of 0.1 M HCl and 0.1 M KOH were prepared from JT Baker DILUT-IT ampoules using freshly degassed Milli-Q purified water. Precise acid concentration was determined by titration of a sodium tetraborate solution to the Methyl Red endpoint. Precise base concentration was determined by titration of a potassium hydrogen phthalate solution to the phenolphthalein endpoint. Stock solutions of EDTA were obtained by dissolving disodium EDTA (Fisher) in freshly degassed Milli-Q water. Precise ligand concentration was determined by performing potentiometric titrations of the ligand solution (pH 3.5 to 8.0 and back to 3.5) in triplicate and solving for total moles of ligand using the program Hyperquad [23], by calculating the buffering capacity of the solution based on published protonation constants [25]. Stock solutions of ferric ion were obtained by dissolving solid $FeCl_3 \cdot 6H_2O$ in standardized 0.1 M HCl. The actual ferric ion concentration was determined by titration with a standardized EDTA solution to the Variamine Blue endpoint [32].

4.8.2 Protonation constants. The protonation constants of 5LIOHOPO$_2$TAM were determined by potentiometric titration. Solutions were assembled from a weighed portion of ligand and the supporting electrolyte solution, with resulting ligand concentrations between 0.2 and 0.5 mM. A pH range from 4.5 to 11 was used. The solutions were incrementally perturbed by the addition of either acid (HCl) or base (KOH) titrant, followed by a 90-s time delay for equilibration. All titrations were conducted in pairs: first a forward titration from low to high pH, then a reverse titration back to low pH. The data for the two titrations comprising each experiment were pooled for calculation of formation constants. An average of 60–90 data points were collected in each pair of titrations, each data point consisting of a volume increment and a pH reading; the titrations were repeated three times to provide at least 180 data points for final refinement of the ligand pK_as. Refinement of the protonation constants was accomplished using the program Hyperquad [23], which allowed simultaneous refinement of the data from multiple titration curves. The four proton association constants were refined to be $\beta_{011} = 9.68$, $\beta_{012} = 17.13$, $\beta_{013} = 23.67$ and

$\beta_{014} = 29.48$, corresponding to pK_as of 5.81(2), 6.54(2), 7.45(2) and 9.69(2). The global σ value for the refinement was 0.083, and the largest correlation coefficient between two protonation constants was 0.79. In the course of the refinement, the molar amount of ligand used in each titration was refined; the average molecular weight calculated from these molar amounts corresponded closely with that determined by elemental analysis.

4.8.3 Batch EDTA competition titrations. Bulk titration solutions were assembled from the constituent reagents in ratios determined previously by modeling using estimated formation constants and the modeling program Hyss [33,34]. A trial titration solution was assembled and systematically varied in pH to confirm the appropriate conditions. The following concentration ranges were used for iron, ligand and EDTA in the competition titrations: Fe 0.08–0.14 mM; ligand 0.09–0.15 mM; EDTA 0.8–1.5 mM. In every case, the EDTA and ligand were present in at least 5% excess over the iron to prevent formation of insoluble iron species. For each titration, 12 aliquots of the bulk solution were removed with a volumetric pipet and stored in plastic centrifuge tubes. The pH of each aliquot was adjusted individually between pH 3.0 and 5.3 using acid (HCl) or base (KOH) titrant. At the lower pH end of the titration, the colorless iron–EDTA complex dominated, but as the pH was raised, the charge-transfer bands for the ligand–iron complex could be seen growing in at 410 and 530 nm. The aliquots were allowed to equilibrate at 25°C for at least 48 h, at which time the final pH was determined and a UV–visible spectrum over at least 80 different wavelengths between 400 and 700 nm was taken of each aliquot. All absorbance measurements used for calculation of formation constants were less than 1.05 absorbance units. The data were imported into the refinement program pHab [35] and analyzed by nonlinear least-squares refinement. The previously determined ligand protonation constants were included as constants, as were the literature values for the protonation and iron complex formation constants of EDTA [25]. Factor analysis of the collected spectra during refinement indicated the presence of a single absorbing species in solution, and this species was modeled as the FeL^- complex. Refinement of the data with this model gave a final value of $\log \beta_{110} = 32.1(1)$.

4.9 *X-ray crystallography*

Crystals of potassium Fe-5LIOHOPO$_2$TAM crystallized in the monoclinic space group $P2_1/c$ as dark purple blocks grown from a DMF solution diffused with diethyl ether. Crystals of potassium Fe-5LIHOPO$_2$TAM crystallized in the triclinic space group $P\bar{1}$ as dark purple blocks grown from a DMF/ethanol solution diffused with diethyl ether. Crystals of potassium Fe-6LIHOPO$_2$TAM crystallized in the monoclinic space group $I2/a$ as dark purple plates grown from a DMF solution diffused with diethyl ether.

Selected crystals of each compound were mounted in Paratone N oil on quartz capillaries and frozen in place under a cold N_2 stream (110–150 K, maintained throughout data collection). The crystallographic data sets were collected on a Siemens SMART X-ray diffractometer equipped with a CCD area detector using Mo Kα radiation ($\lambda = 0.71072$ Å, graphite monochromator). An arbitrary hemisphere of data was collected for each crystal using ω scans of 0.3° per CCD area detector frame and a total measuring time of 10 to 35 s each (measuring time constant for each crystal).

Table 1. Iron complex crystal data.

Compound	Fe[5LIOHOPO$_2$TAM]	Fe[5LIHOPO$_2$TAM]	Fe[6LIHOPO$_2$TAM]
FW	950.8	918.8	978.38
Temp, K	114	143	137
Max 2θ	49.44	49.98	49.48
Crystal system	Monoclinic	Triclinic	Monoclinic
Space group	$P21/c$	$P\bar{1}$	$I2/a$
Unit cell dimensions			
a, Å	20.6200(19)	12.4679(16)	28.1875(29)
α,°	90	78.163(2)	90
b, Å	9.2365(9)	12.7498(16)	15.6457(16)
β,°	113.406(1)	69.841(2)	90.080(2)
c, Å	23.8669(22)	15.1475(19)	22.6837(23)
γ,°	90	89.671(2)	90
Volume, Å^3; Z	4171.58(74); 4	2206.78(44); 2	10 003.81(1.67); 8
Calc. density, g/cm^3	1.51	1.38	1.30
Crystal size (mm)	$0.40 \times 0.30 \times 0.30$	$0.35 \times 0.30 \times 0.20$	$0.40 \times 0.35 \times 0.10$
Abs. coefficient, μ, mm^{-1}	0.52	0.49	0.45
Reflections collected	17656	11158	21799
Independent reflections	6909	7086	8253
Data-to-parameter ratio	11.8	12.3	13.8
Goodness-of-fit on F^2	1.020	1.028	0.960
Final R indices ($I > 2\sigma(I)$)			
$R1$	0.0470	0.0656	0.0554
$wR2$	0.1268	0.1777	0.1448
R indices (all data)			
$R1$	0.0557	0.0873	0.0923
$wR2$	0.1345	0.1968	0.1592
Largest diff. peak and hole, e Å^{-3}	0.73 and −0.68	0.65 and −0.61	0.67 and −0.53

The intensity data to a maximum 2θ range of ~50° (specific 2θ different for each crystal) were integrated using SAINT with box size parameters of $1.6 \times 1.6 \times 0.6$ [36]. The data were corrected for Lorentz and polarization effects. An empirical absorption correction for each crystal was based on the measurement of redundant and equivalent reflections using an ellipsoid model for the absorption surface and was applied using SADABS [37]. Equivalent reflections were merged, and the space groups were determined using XPREP [38] on the basis of lattice symmetry and systematic absences. When two space groups were possible, the final choice was made based on the successful solution and refinement of the structures.

The structures were solved by direct methods (SHELXS-86) [39]. After most of the atoms had been located, the data set was refined using the SHELXTL-97 software package [38]. All nondisordered nonhydrogen atoms were refined anisotropically. Unless otherwise noted, hydrogen atoms were assigned to idealized positions. Additional experimental details for each structure are summarized in table 1.

Acknowledgments

We thank Dr Fred Hollander and Dr Allen Oliver for assistance with the X-ray structure determinations, Dr Seth Cohen, Dr Jide Xu and Emily Dertz for helpful discussions, and Dr Anne Gorden for assistance in editing. This work was supported

by the National Institutes of Health (NIH Grant DK32999, with continuing support from DK57814).

References

[1] N.C. Andrews. *Rev. Clin. Exp. Hematol.* **4**, 283 (2000).
[2] N.C. Andrews. *New Engl. J. Med.* **341**, 1986 (1999).
[3] C. Hershko. *Rev. Clin. Exp. Hematol.* **4**, 337 (2000).
[4] R.A. Yokel, A.M. Fredenburg, P.W. Durbin, J. Xu, M.K. Rayens, K.N. Raymond. *J. Pharm. Sci.* **89**, 545 (2000).
[5] G. Rivkin, G. Link, E. Simhon, R.L. Cyjon, J.Y. Klein, C. Hershko. *Blood* **90**, 4180 (1997).
[6] R.J. Bergeron, R.R. Streiff, W. King, R.D. Daniels Jr, J. Wiegand. *Blood* **82**, 2552 (1993).
[7] R.J. Bergeron, J. Wiegand, G.M. Brittenham. *Blood* **99**, 3019 (2002).
[8] W. Przychodzen, A. Chimiak, *Pol. J. Chem.* **69**, 1729 (1995).
[9] C.G. Pitt, Y. Bao, J. Thompson, M.C. Wani, H. Rosenkrantz, J. Metterville. *J. Med. Chem.* **29**, 1231 (1986).
[10] P.W. Durbin, B. Kullgren, J. Xu, K.N. Raymond. *Health Phys.* **72**, 865 (1997).
[11] P.W. Durbin, B. Kullgren, S.N. Ebbe, J. Xu, K.N. Raymond. *Health Phys.* **78**, 511 (2000).
[12] L.C. Uhlir, P.W. Durbin, N.L. Jeung, K.N. Raymond. *J. Med. Chem.* **36**, 504 (1993).
[13] S.M. Cohen, J. Xu, E. Radkov, K.N. Raymond, M. Botta, A. Barge, S. Aime. *Inorg. Chem.* **39**, 5747 (2000).
[14] S.M. Cohen, B. O'Sullivan, K.N. Raymond. *Inorg. Chem.* **39**, 4339 (2000).
[15] J. Xu, B. Kullgren, P.W. Durbin, K.N. Raymond. *J. Med. Chem.* **38**, 2606 (1995).
[16] Y. Nagao, T. Miyasaka, Y. Hagiwara, E. Fujita. *J. Chem. Soc. Perkin Trans.* 1, 183 (1984).
[17] J.R. Telford, K.N. Raymond. In *Comprehensive Supramolecular Chemistry*, Vol. 1, pp. 245–266, J.L. Atwood, J.E.D. Davies, D.D. MacNicol, F. Vogtle (Eds), Elsevier Science Ltd, Oxford (1996).
[18] J. de Abajo, J.G. de la Campa, E. Riande, J.M. Garcia, M.L. Jimeno. *J. Phys. Chem.* **97**, 8669 (1993).
[19] G.A. Jeffrey (Ed.). *An Introduction to Hydrogen Bonding*, Oxford University Press, Oxford, UK (1997).
[20] T.B. Karpishin, T.D.P. Stack, K.N. Raymond. *J. Am. Chem. Soc.* **115**, 182 (1993).
[21] D.L. Kepert. *Inorganic Stereochemistry*, Springer-Verlag, Heidelberg (1982).
[22] B.A. Borgias, S.J. Barclay, K.N. Raymond. *J. Coord. Chem.* **15**, 109 (1986).
[23] P. Gans, A. Sabatini, A. Vacca. *HYPERQUAD2000*, Leeds, UK and Florence, Italy (2000).
[24] A.E. Martell, R.J. Motekaitis. *Determination and Use of Stability Constants*, VCH, New York (1988).
[25] R.M. Smith, A.E. Martell. *Critical Stability Constants*, Vols 1–4, Plenum, New York (1977).
[26] J. Xu, S.J. Franklin, D.W. Whisenhunt, K.N. Raymond. *J. Am. Chem. Soc.* **117**, 7245 (1995).
[27] D.M.J. Doble, M. Melchior, B. O'Sullivan, C. Siering, J. Xu, K.N. Raymond. *Inorg. Chem.* (in press).
[28] A.R. Johnson, B. O'Sullivan, K.N. Raymond. *Inorg. Chem.* **39**, 2652 (2000).
[29] J. Xu, B. O'Sullivan, K.N. Raymond. *Inorg. Chem.* **41**, 6731 (2002).
[30] P. Gans, B. O'Sullivan. *Talanta.* **51**, 33 (2000).
[31] *LABVIEW*, 5.0.1 ed., National Instruments Corp., Austin, TX.
[32] K. Ueno, T. Imamura, K.L. Cheng. *Handbook of Organic Analytical Reagents*, 2nd edn, CRC Press, Boca Raton, FL (1992).
[33] L. Alderighi, P. Gans, A. Ienco, D. Peters, A. Sabatini, A. Vacca. *Coord. Chem. Rev.* **184**, 311 (1999).
[34] L. Alderighi, P. Gans, A. Ienco, D. Peters, A. Sabatini, A. Vacca. *HYSS*, Leeds, UK and Florence, Italy (1999).
[35] P. Gans, A. Sabatini, A. Vacca. *Ann. Chim.* (*Rome*), **89**, 449 (1999).
[36] *SAINT, SAX Area-Detector Integration Program*, 4.024 ed., Siemens Industrial Automation, Inc., Madison, WI (1994).
[37] *SMART Area-Detector Software Package*, Siemens Industrial Automation, Inc., Madison, WI (1994).
[38] *SHELXTL, Crystal Structure Analysis Determination Package*, 5.10 ed. Siemens Industrial Automation, Inc., Madison, WI (1997).
[39] G.M. Sheldrick. *Acta Crystallogr., Sect. A*, **46**, 467 (1990).